AERODYNAMIC OPTIMISATION OF AN AEROFOIL'S SHAPE COUPLED WITH AN OPTIMISATION OF ITS INNER STRUCTURAL TOPOLOGY

Isaac Gibert Martínez
isaac.gibert.martinez@tecnico.ulisboa.pt

Instituto Superior Técnico, Universidade de Lisboa, Portugal

January 2021

Abstract

The overall purpose of the work lies on the coupling of two optimisation procedures for the main fields of study, the aerodynamics and the topology layout of an aerofoil, by means of different open-source resources, SU2 and *Calculix* respectively, capable to provide robust and efficient simulations in both studied fields. The RAE 2822 geometry used to test the open-source software is the 2D benchmark case for transonic viscous aerodynamic profiles, with the wing-box as a geometric constraint. The aerofoil has been initially drag-minimised for two different configurations, Mach number $M = 0.729$ at an angle of incidence $\alpha = 2.31^\circ$ and $M = 0.730$ at $\alpha = 2.79^\circ$ while setting a fixed lift constraint using the *Free-Form Deformation* methodology; afterwards, the *Bi-directional Evolutionary Topology Optimisation* was applied to the optimised shape inside the *Calculix* environment. A migratory procedure of the obtained data was required by the topology analysis from the aerodynamic output so as to apply the pressure loads on the aerofoil's surface as concentrated loads. Then, a sequential coupling strategy was followed since the aerodynamic optimisation represented an improvement to the general pressure distribution and, subsequently, it represented a diminishing of two orders of magnitude below for the loading state and the final displacements. Conclusively, the sequential coupling has proved to be beneficial as the aerodynamic improvement allowed the inner layout to redistribute in a more efficient way, reducing its inner surface to 25% of the original one, while providing a robust and structurally sound design.
Keywords: Aerodynamic Optimisation, CFD, RAE 2822, Topology Optimisation, Calculix, SU2

I Introduction

The term '*efficiency*' in the aeronautical industry is gaining more and more weight every passing year as, apart from leading a transversal innovation across all the engineering fields, it is always trying to reach the excellence and perfectionism of its science. Apart from performance efficiency the new aircraft designs have to cope with two of the hardest enemies of the human specie and the world itself have had to face, the climate change and the environmental resources management.

Nevertheless, it is not explicitly necessary to rearrange the actual concept of an aircraft so as to provide more efficient designs. Within them, the most renowned areas of improvement are found in the geometry optimisation features [1] [2], combustion and gas exhaust systems [3], and the weight reduction target [4].

In this work two optimisation approaches will be followed and applied to the *RAE 2822* aerofoil considering the study to be bi-dimensional. Moreover, it has been decided to apply a geometric constraint in the study, the one based on the wing-box position in the aerofoil. Both approaches pretend to reduce the fuel consumption but following two alternative paths. One of them is optimising the aerodynamics of the aerofoil by modifying its geometry for specific flow conditions, thus reducing the required thrust power to provide the motion to the aircraft, while the other procedure works in rearranging the material inside the aerofoil aiming at the highest stiffness-to-weight ratio and, therefore, the lowest lift force required to fly the aircraft.

To do so, a sequential approach has been followed. This means that the optimisations are not carried out in parallel. Instead, the aerofoil shape is initially redesigned recurring to Aerodynamic Shape Optimisation, followed by a Topology Optimisation of its inner structure.

Finally, the optimal aerodynamic results joined with the inner, more efficient, structural layout will be analysed, filtering the positive output gained from the study and proposing new future milestones for the

community.

II Background

The present work is based on a *Computational Fluid Dynamics* approach towards the aerodynamics and the shape optimisation of the geometry, followed by a topology optimisation of the inner structure of the aerofoil. Hence, a brief introduction of the governing equations and their numerical implementations is presented.

A. Aerodynamics: Governing Flow Equations

The flow's behaviour is modelled by an approximate methodology, the so called *Reynolds Averaged Navier-Stokes* (*RANS*) equations, specifically using the turbulent model provided by *Spalart* and *Allmaras* [5], because of its simplicity and accuracy. The final formulation for the *RANS* model is described in a differential form [6] as follows:

$$\begin{cases} \dfrac{\partial(\mathbf{U})}{\partial t} + \nabla\cdot\mathbf{F}^c - \nabla\cdot\mathbf{F}^v - \mathscr{Q}_\phi = \Re(\mathbf{U}) & \text{in } \Omega, \quad t{>}0, \\ \mathbf{u}_\Omega = 0 & \text{on } S, \\ \dfrac{\partial T}{\partial n} = 0 & \text{on } S, \\ (W_+) = W_\infty & \text{on } \Gamma_\infty \end{cases} \tag{1}$$

where $\mathbf{U}$ are the conservative variables given by $\mathbf{U} = \{\rho, \rho\mathbf{v}, \rho E\}$, being ρ the density, $\boldsymbol{v}$ the flow's speed and E the internal energy of the system respectively, $\Re$ is the numerical residual and the respective convective and viscous fluxes $(\nabla\cdot\mathbf{F}^c, \nabla\cdot\mathbf{F}^v)$, Ω is the tridimensional domain separated from a far-field component Γ_∞ and its flow conditions W_∞, an adiabatic wall boundary S which represents the aerofoil body and $\mathscr{Q}$ represents the source term.

B. Gradient Based Methodology: Discrete Adjoint Approach for the aerodynamic optimisation

In each of the volumes cells of the CFD domain there is a certain number of variables that shape the final result of the setup. By performing small perturbations to those variables, it is possible to evaluate sensitives that these have on a studied objective function. In aerodynamics, it is common to use the *Gradient-based* optimisation algorithm to make use of sensitivity analysis [7][8], specially when using the adjoint method. This procedure can deal with a large number of input variables to work with. To begin with, a specific total variable must be selected for the study, called the objective function L, for instance, lift, drag or moment coefficients. L depends on the flow variables of the study (solution), u, and the design variables (or parameters), D, which represent the modifications in the original state. Then, the sensitivity formulation is defined as:

$$\frac{dL}{dD} = \frac{\partial L}{\partial D} + \frac{\partial L}{\partial u}\frac{\partial u}{\partial D} \tag{2}$$

Sensitivity is basically the output obtained when analysing the effect that an independent parameter has on a dependant one by means of its uncertainty (in this case, the difference to an original value). By compiling all sensitivities in a matrix format, one produces the Jacobian matrix of a given function L to a set of inputs D [7]. The flow solution must be constrained after the sensitivity analysis as it is required to be converged.

From this point, once the sensitivity formulation has been described, the adjoint method is applied [9]. Defining the adjoint variables matrix as Ψ, the adjoint solution is only dependant of the objective function L and not from the design parameters D and that there is an adjoint solution for each objective function that has been defined. Then, a linear system is obtained which complexity depends on the number of the design variables:

$$\left[\frac{\partial R}{\partial u}\right]^T \Psi = -\left[\frac{\partial L}{\partial u}\right]^T \tag{3}$$

and embedding it to the final form of the sensitivity formulation (or total derivative), the final form is:

$$\frac{dL}{dD} = \frac{\partial L}{\partial D} + \Psi^T\frac{\partial R}{\partial D} \tag{4}$$

C. Parametrisation technique: Free-Form Deformation

In this work, the *Free-Form Deformation* (FFD) methodology is used. It is a technique developed by *Sederberg* in [10] to model solids and has its recognition not only due to its versatility, but also since it does not manipulate directly the geometry of the object, in opposition of other parametrisation techniques, but the lattice of a certain space in the domain where the object is embedded. For two-dimensional cases the box looks like a rectangle and like a cube for 3D cases.

The formulation deals with some vectorial and spatial embedding and deformations. If a point $\boldsymbol{X}$ with coordinates (x_1, x_2, x_3) is embedded into a new reference frame ***s, t, p***, ends up being defined as (5):

$$\mathbf{X} = X_0 + s\mathbf{S} + t\mathbf{T} + p\mathbf{P} \tag{5}$$

From this point, the FFD box must be constrained and defined in the new coordinates as well as the embedded geometry. The original and unperturbed control points, ($P^0_{l,m,n}$), then can be defined. The next step is to introduce the deformation by a parameter $\mu_{l,m,n}$ whose dimension considers the 3-axis movement. From this point, every control point is deformed by the latest parameter such as:

$$\mathbf{P}_{l,m,n} = \mathbf{P}^0_{l,m,n} + \mu_{\mathbf{l,m,n}} \tag{6}$$

meaning then that the final parametrisation is defined as:

$$\mathbf{X}_{ffd} = \sum_{l=0}^{L}\sum_{m=0}^{M}\sum_{n=0}^{N} b^{L,M,N}_{l,m,n}(s,t,p)P_{l,m,n}\left(\mu_{l,m,n}\right) \tag{7}$$

D. Optimisation Framework

Aerodynamic optimisation is the process of providing the most efficient solution for a given objective function (f), while coping with a set of inequality (g) and equality (h) constraints by a set of design variables . A general view of the problem can be defined as [11]:

$$\begin{aligned} &\text{Minimise} \quad f(\mathbf{D}) \quad \leftarrow \quad \textit{Objective function w.r.t. } \boldsymbol{D} \\ &\text{Subject to} \quad \begin{cases} g_j(\mathbf{D}) \le 0 & j = 1, m \\ h_k(\mathbf{D}) = 0 & k = 1, n \end{cases} \end{aligned} \tag{8}$$

E. Solid Mechanics: Governing Material Equations

Regarding the science behind the case of study, the aerofoil is going to be considered to behave inside the elastic region of the material, specifically inside the linear region, then, it will follow the Hooke's law, which implies a proportional relation between the stresses (σ) and the correspondent strains (ϵ) by means of the constitutive matrix C.

$$\sigma_{ij} = C_{ijkl}\epsilon_{kl} \tag{9}$$

The stresses can be written as the Cauchy stresses that follows the Hooke's law form is expressed as follows [12]:

$$\sigma = \lambda tr(\epsilon)\mathbf{I} + 2\mu\epsilon \tag{10}$$

where $\boldsymbol{I}$ is the rank-2 identity tensor while λ and μ are the *Lamé* constants written as a function of the bulk modulus K, and shear modulus G. As Lamé constants are not given for each of the materials, equation (10) can be arranged by using the *Young's* modulus E and the *Poisson* ratio ν relation (eq. (11)) with the previous constants. Thus, the final expression is the one from equation (12):

$$\begin{cases} \lambda = \dfrac{E\nu}{(1+\nu)(1-2\nu)} \\ \mu = \dfrac{E}{2(1+\nu)} \end{cases} \tag{11}$$

$$\sigma = \frac{E\nu}{(1+\nu)(1-2\nu)}\,tr(\epsilon)\mathbf{I} + \frac{E}{(1+\nu)}\epsilon \tag{12}$$

F. Topology Optimisation.

For the topology optimisation, the *Bi-directional Evolutionary Structural Optimisation* (*BESO*) algorithm as provided in [13] is used due to its usual applicability for these types of problems. This algorithm is in fact an improvement procedure from the development made by [14] for the *Evolutionary Structural Optimisation*. The main difference between the procedures named above is that the former not only removes mass of the geometry, but it also can add it.

The *BESO* methodology removes the low-stressed areas of a domain which is understood to be inefficient and adds material when it is strictly necessary to provide a higher stiffness to the structure. For the initial proposal, a 'hard-kill' method was used, which uses a rejection/addition ratio, c_{rr}/c_{ar}, to mark as removable/immovable the ones below it. This rejection criteria uses the von Mises stress of a cell, σ^{vM}_e, and compares it with a threshold, σ^{vM}_{max}, which could be a maximum or a prescribed value, thus:

$$\begin{cases} \sigma^{vM}_e \le c_{rr}\sigma^{vM}_{max} \rightarrow \text{Element removal} \\ \sigma^{vM}_e \ge c_{ar}\sigma^{vM}_{max} \rightarrow \text{Element addition} \end{cases} \tag{13}$$

The followed procedure tries to find the stiffest geometry for a given volume, one of the most common tendencies for the topology optimisation. The objective is to minimise the strain energy (thus the compliance) for a given volume fraction, by attributing material or void to each element of a previously defined mesh of the structure. A standard formulation of this problem is as follows:

$$\begin{aligned} &\text{Minimise} \quad C = \frac{1}{2}\mathbf{f}^T\mathbf{u} = \frac{1}{2}\sum_{i=1}^{N} {u_i}^T K u_i \\ &\text{Subject to} \quad V^{Fin} - \sum_{i=1}^{N} V_i\chi_i = 0 \\ &\qquad\qquad \chi_i \in \{0,1\} \end{aligned} \tag{14}$$

where C is the mean compliance of the structure and $\boldsymbol{u}$ and $\boldsymbol{f}$ are the displacement and load vectors respectively, V^{Fin} denotes the target volume fraction, V_i, is the volume of each element, N is the total amount of elements and χ is the binary description of the presence of mass, being 0 a void and a 1 a filled state.

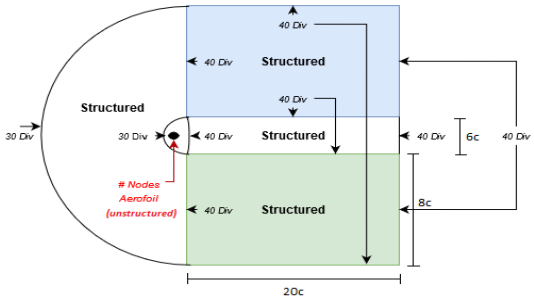

Figure 1: Grid accounted for the extraction of the results.

III Implementation

A. Aerodynamics

i. CFD Simulation Framework

The selected geometry is the *RAE 2822* aerofoil, designed specifically for transonic regimes where a shockwave is present, specially at the Reynolds number for which the simulation is going to be established ($Re = 6.5e^6$). This Reynolds number is selected due to the availability of experimental data [15] to validate the obtained results. Then, the flow conditions of the case study are defined by the *Reynolds* and *Mach* number, $Re = 6.5 \cdot 10^6$ and $M = 0.729$ respectively, with an angle of incidence of $\alpha = 2.31°$.

The mesh has been designed considering: the constraints applied at the boundaries of the domain such that they do not have a noticeable influence on the results [16] [17]; mesh quality parameters (*e.g.* element's orthogonality and flow alignment); the tracking of the y^+ magnitude so as to represent in the study the present phenomena in the boundary layer; and by setting a far-field boundary condition.

From this point, a C-type mesh domain with 53492 elements was generated, dividing the layout into 5 regions: 4 structured regions including the more external parts from the aerofoil's location and the wake; and an unstructured distribution surrounding the studied geometry. Moreover, a mesh refinement was applied at the boundaries of the aerofoil, converting the grid into a structured distribution and densifying the number of variables inside the boundary layer aiming at a wall-grid spacing of $1 \cdot 10^{-6}$c. A general view of the layout can be observed in Figures (1) and (2).

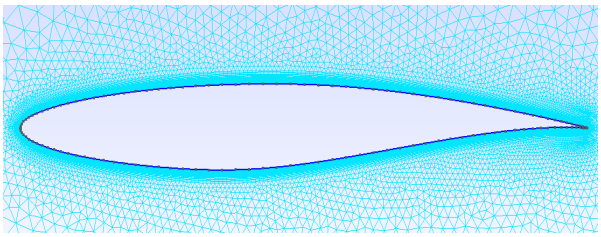

Figure 2: View of the boundary layer refinement.

Thereafter and by using the open-source CFD tool *SU2*, the results can be extracted in terms of pressure coefficient distribution. In Figure (3) an accurate similitude between both methodologies [15] can be noted.

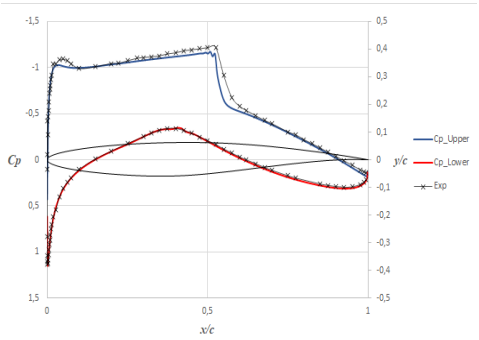

Figure 3: Pressure coefficient of the simulation and the one from the experimental setup.

Concerning the lift and drag aerodynamic coefficients, in Table 1 are presented the numerical results, as well as the experimental ones.

Table 1: Comparison between the numerical and the experimental results for the *RAE 2822* aerofoil

	Cl	*Cd*
Present Work	0.7164	137.4
Experimental Work [15]	0.7436	127.0

The selected mesh has been considered by means of a trade-off between the computational costs the CFD simulation involves and the academic purpose of the work. The error in the lift coefficient compared to the experimental setup is low (**3.66%**) but it is possible to notice yet the difference in drag counts, approximately a 7%, but, for the purpose of this work and the limited interval of available time, it is considered to be acceptable, knowing that more accurate results could be obtained then by using finer meshes.

ii. Aerodynamic Shape Optimisation

After the CFD environment has been set up, the optimisation framework is defined. *SU2* software uses the *Sequential Least SQuares Programming* (SLSQP) module from *SciPy* library of Python for the minimisation procedure of a given objective function. By coupling the open-source packages *NumPy* [18] and *SciPy* [19] the resulting optimisation procedure in *SU2* is numerically and computationally efficient and robust.

The idea behind the process comes from a modification of the *Lagrangian* multipliers for an optimisation process, the Karush-Kuhn-Tucker [20], and provides a *global optimal* by satisfying the conditions build by the objective function, the design variables and the equality and inequality constraints. The solver will be testing new geometries until convergence criterion has been reached.

The main goal of the project was to optimise the aerofoil by means of its efficiency (lift-to-drag ratio). However, the test gave as an output only a **0.15%** of improvement. This means that the aerofoil, for this specific flow conditions and wing-box constraint, is quite optimised. In order to explore the potentiality of the aerodynamic shape optimisation, two case studies were defined. Both aiming at drag minimisation of the same constrained aerofoil for a constant lift coefficient at different angles of attack. In Table 2 are shown the initial values of *Cl* and *Cd* for the two studied cases.

Table 2: Case studies for the *RAE 2822* aerofoil analysed and optimised in the work.

	Initial *Cl*	Initial *Cd*
$Re = 6.5 \cdot 10^6$; $M = 0.729$; $\alpha = 2.31°$	0.7164	137.4
$Re = 6.5 \cdot 10^6$; $M = 0.730$; $\alpha = 2.79°$	0.8030	183.6

B. Adjoint Methodology

For the aerodynamic shape optimisation, the aerofoil must fit inside the designed deformation box without intersecting any of the control points nor the connecting lines but the closer, the better. In that way, the deformation of the control nodes would have more influence in the geometry closer to it. The *RAE 2822* shape must consider the presence of the wing-box constraint. Usually it is considered to be located between *0.25c - 0.75c*, therefore, the control points in this interval will not serve as a design variables as no movement or deformation can be applied to them. In Figure (4), the *RAE 2822*'s wing-box is defined in red.

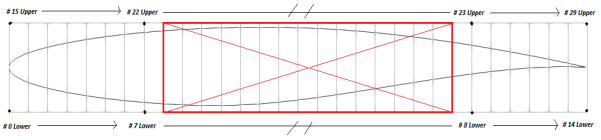

Figure 4: Control Points identification

C. Solid Mechanics

Once the aerodynamic optimisation results are obtained, the pressure distribution along the surface of the aerofoil is an input for the *Finite Element Methodology* (FEM). The structural layout shown in Figure (5) refers to the selected design for the wing-box structure and the skin of the aerofoil which is, afterwards, going to be used as a constraint for the topology analysis. Firstly, a skin thickness of 0.002c is imposed to the geometry and, secondly, a thickness-related constraint of *0.008c* for the wing-box geometry conservation in the topology analysis is added.

Figure 5: Graphical representation of the RAE 2822 case of study complemented with the aerofoil and wing-box skins.

The load applied to the structure is the pressure distributed throughout the aerofoil surface. This load is given by *SU2* which provides data for each node of the surface mesh as an output. A pre-processing analysis should be done to translate the output file obtained by *SU2* to the one read by the *Calculix* software.

As the pressure was discretised in the nodes, the loads should follow the same behaviour. Therefore, the load should be applied to the node where its correspondent pressure value was obtained. To do so, the second space variable is defined using the initial geometry lines between nodes. By coupling the halves of the previous segment and the following one coming from

the primary geometry, a balanced and accurate representation is achieved. In addition, the pressure value it is not applied then in the node, but in the new formed line following the direction of its normal vector. Then, the sign of the vectorial force depends on the magnitude of the pressure, being towards the inner structure when the pressure is positive and outwards when the pressure is negative. This process is illustrated in Figure (6).

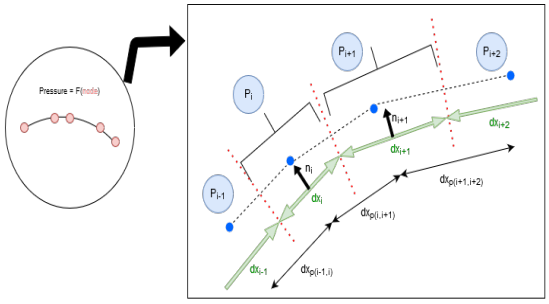

Figure 6: Methodology used to apply concentrated loads from discrete pressure values.

In Figure (6), initial nodes are marked in blue and the geometry is represented by black dashed lines. Then, the distance between nodes is also provided with the variable $dx_{p(node1,node2)}$. The pre-processing before the FEM analysis consists in dividing the initial segments in their mid-point, as seen with the dotted lines in red, subsequently there are the new segments which connect the mid-nodes and save the information in the dx_i variable, which has also its own normal vector $\hat{n}_i$. Therefore, and showed by the brackets, the pressure value from the specific node is applied along that surface defined by $(dx_i \times 1c) \cdot \hat{n}_i$. A representation of this methodology result is shown in Figure (7).

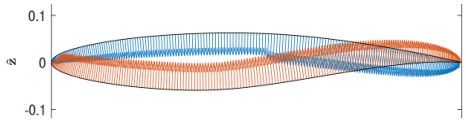

Figure 7: Pressure field translated into loads for the RAE 2822 case of study.

Initially, and because of the mesh dependence feature, the results vary in distribution along with the mesh quality and quantity, so the first task carried out was to find a mesh distribution able to provide consistent results and practically not influenced by the number of nodes. Different meshes were built and their results in terms of von Mises stresses, σ_{VM}, and displacements d, are shown in Figure (8). Because of the acceptable computational cost involved and a better expected accuracy in the results, the highest density mesh, with 77144 elements, has been selected for the study.

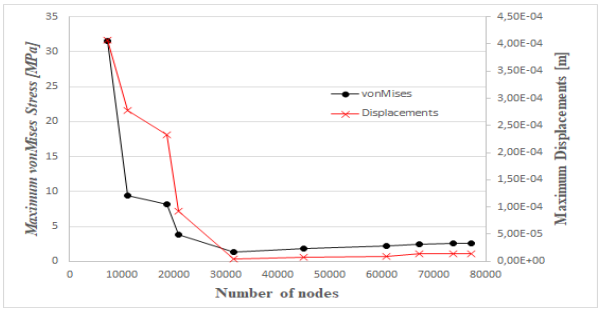

Figure 8: Structural variables' evolution with the number of nodes.

D. Topology Optimisation

The topology study conditions are initially defined by the minimisation of the compliance-to-weight ratio (maximisation of the stiffness-to-weight ratio), the specific constraints of the case study and the avoidance of instabilities such as the checkerboard layout [21]. Therefore, a removal rate of 3 was considered to be adequate, thus each iteration the solver provides a 3% state lighter than the previous.

The aim of the procedure is to evaluate the different layouts given for a set of weight constraints (Figure (9)), which were defined to be: 50%, 35%, 25% and 10%. Not only the material modification rates are important but also the values of the magnitudes which they apply for. For instance, the material removal value has been set to 4% of the total mass while the additive one is 1%, therefore, the stated 3% general removal state. The sensitivity filter used is the one defined by *simple*, which uses the neighbouring cells as an averaging magnitude method that avoids the *checkerboard* phenomena. Then, that filter radius ranges from 8-10 times the mesh element size (0.01c). This selected parameters have been extracted by an experimental list of setups, which have provided the meaningful information so as to reach the stated goals of the process.

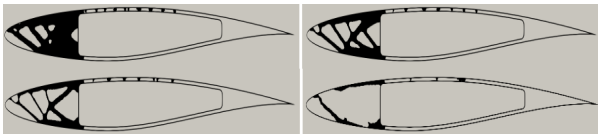

Figure 9: Material layout distribution for the general case study, considering 50%, 35%, 25% and 10% mass constraint reduction targets.

IV Results

A. Aerodynamic Optimisation

As stated previously, two case studies were aerodynamically optimised by fixing the lift coefficient and minimising the produced drag. Moreover, the wingbox area was also set as fixed, thus any shape modifications should appear at the leading and trailing edges.

i. Case 1: $Re = 6.5 \cdot 10^6$; $M = 0.729$; $\alpha = 2.31°$

The optimised solution for the case of study involves small deformations which, despite small, reduced the drag coefficient by **13.9%** as it can be seen from Table 3.

Table 3: Aerodynamic Coefficients for the optimised aerofoil's shape.

Shape	*Cl*	*Cd* counts
Original	0.7164	137.40
Optimised	0.7164	118.23

When analysing the pressure distribution shown in Figure (10), it is possible to observe that even for small modifications in shape the pressure distribution substantially changes. The magnitude of the highest deformation is 0.1%c, thus the sensitivity of the changes in the geometry have significant weight towards the final result. Note that the solver, in order to reduce the drag while constraining the lift, tries to slow down the flow when getting closer to the formation of the shockwave so as to absorb some of the kinetic energy of the flow and, as the counterpart, this speed decrease is adjusted close to the leading edge by providing more curvature, thus a higher pressure gradient.

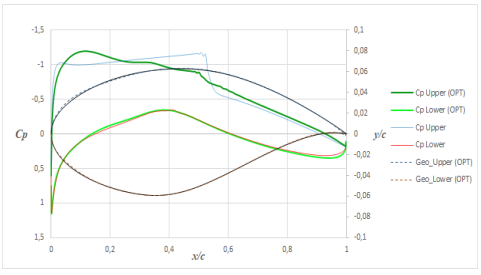

Figure 10: Pressure coefficient comparison.

ii. Case 2: $Re = 6.5 \cdot 10^6$; $M = 0.730$; $\alpha = 2.79°$

For the second case study, in Table 4, it is possible to appreciate a **29.04%** reduction of the drag coefficient, higher than for the previous case. The geometric changes in the leading edge increased while keeping the conditioning of the shockwave's occurance by lowering the speed in that sub-region.

Table 4: Aerodynamic coefficients for the second case optimised aerofoil's shape.

Shape	*Cl*	*Cd* counts
Original	0.803	183.62
Optimised	0.803	130.29

Regarding the pressure coefficient distribution, Figure (11), along the aerofoil, there is a higher peak of suction closer to the leading edge than in Figure (10). As well as in the previous case, the greater magnitude of the modifications of the geometry is in the order of 0.5%c (if the chord was defined as 1 meter, the deformation would be 5 mm) thus is not easily noticed.

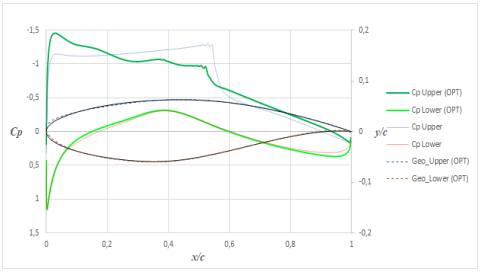

Figure 11: New pressure coefficient distribution comparison for the $\alpha = 2.79°$ case.

B. Structural Results

For the (non-)optimised cases, a completely-filled aerofoil geometry has been studied in terms of the suffered displacements and stresses due to the pressure loading in order to see which was the influence the aerodynamic shape change had in the solid mechanics field. In this section, a visual and numerical comparisons are provided for each of the two studied cases.

i. Case 1: $Re = 6.5 \cdot 10^6$; $M = 0.729$; $\alpha = 2.31°$

When aerodynamically optimising the aerofoil's shape, the stress and displacements distributions inside the aerofoil change completely, not only in magnitudes, as it can be seen in Table 5, but also in its location. In Figure (12) the von Mises stress distribution is compared while the displacements behave in a non-influential interval.

Table 5: Structural parameters comparison between the optimised and the non-optimised aerofoil's geometries.

Geometry	σ_{vM}^{max} $[Pa]$	$\lvert d_{max} \rvert$ $[c]$
Original	$2.63 \cdot 10^6$	$1.47 \cdot 10^{-5}$
Optimised	$7.48 \cdot 10^4$	$1.19 \cdot 10^{-6}$
Decreased to a %	2.85%	8.1%

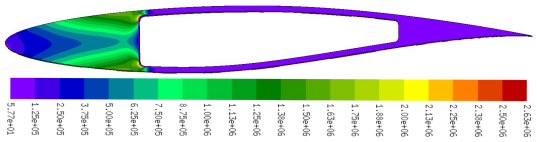

(a)

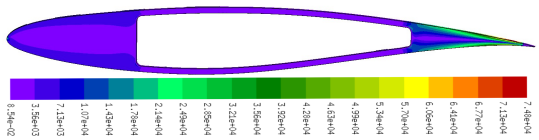

(b)

Figure 12: (a) Von Mises stress distribution for the case study and (b) von Mises stress distribution for the optimisation one.

Regarding the von Mises stresses, the maximum value has substantially decreased in 97%, from 2.63 MPa to 74.8 kPa, while the stress distribution has moved towards the trailing edge, where it has the lowest material density.

i. Case 2: $Re = 6.5 \cdot 10^6$; $M = 0.730$; $\alpha = 2.79°$

An analog feature is reproduced for the second study case (Table 6 and Figure (13)):

Table 6: Structural parameters comparison between the optimised and the non-optimised aerofoil's geometries.

Geometry	σ_{vM}^{max} $[Pa]$	$\lvert d_{max} \rvert$ $[c]$
Original	$2.51 \cdot 10^6$	$1.40 \cdot 10^{-5}$
Optimised	$3.72 \cdot 10^4$	$4.03 \cdot 10^{-7}$
Decreased to a %	1.49%	2.88%

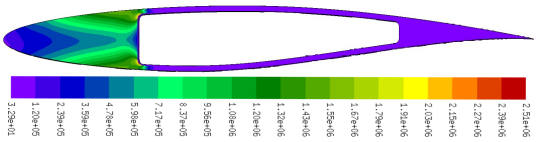

(a)

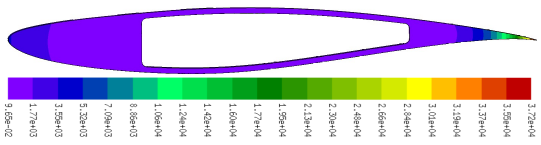

(b)

Figure 13: (a) Von Mises stress distribution for the second case study and (b) von Mises stress distribution for the optimisation one.

The new stress distribution represents a 1.48% of the loading state for the initial case, reaching a maximum value of 37.2 KPa and a displacement of 0.403 μc. It is worth to note how very small changes in the surface of the aerofoil when optimising the geometry have a great influence on the stress distribution.

C. Aerodynamic and Structural Optimisations

In terms of the purpose of this work, the sequential approach has been selected, as it provides insightful information about the benefits the coupling has on the future performance of the case study. Therefore, the aerodynamics subject was developed initially and followed by the structural one, both including their respective optimisation procedures. Once the optimal solution is found by the solver, the output can be analysed. In Figure (14), there is a graphical representation of the followed methodology.

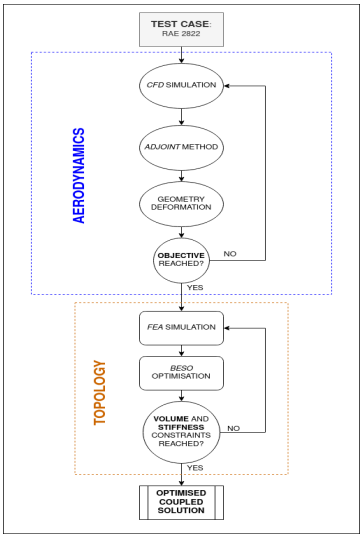

Figure 14: Sequential approach algorithm followed in this work.

i. Case 1: $Re = 6.5 \cdot 10^6$; $M = 0.729$; $\alpha = 2.31°$

Regarding the optimised geometries given by the topology optimisation solver, the 25% weight constraint (Figure (15)) seems to be an ideal shape for the design as, it is noticeably efficient in terms of mass reduction but not as simple and fragile-looking as in lighter cases. In order to avoid ruptures or unexpected failures, it is better to reinforce the general layout even though the final weight is higher.

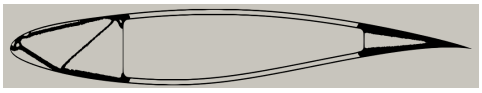

Figure 15: Weight reduction target: 25%.

It is worth to point out how the Failure index (FI) of Figure (16a) is two orders of magnitude lower than in the non-aerodynamically optimised case, meaning that, from a first approach, the structure should perfectly withstand the loading state. In terms of stresses (Figure (16b)), the structure finds itself in a more relaxed situation, because the pressure loads are softened when aerodynamically optimised and also absorbed in the leading edge region due to the appearance of new material. Apart from this latest statement, note how the inner stresses have a higher value than in the completely material-filled aerofoil (but in the same magnitude's interval), as expected since the main purpose of the topology optimisation is to redistribute the loads towards specific regions of the geometry while removing the unnecessary ones.

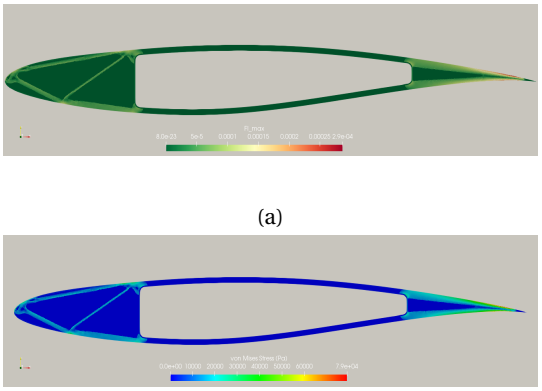

(a)

(b)

Figure 16: (a) Failure index distribution and (b) von Mises stress distribution for the optimisation of the case study for a 25% mass reduction.

ii. Case 2: $Re = 6.5 \cdot 10^6$**;** $M = 0.730$**;** $\alpha = 2.79°$

Aiming at higher modifications in the geometry, a second case study was selected, in which the flow conditions were modified. The reason behind this new strategy is to translate into topological modifications of the inner structure of the aerofoil.

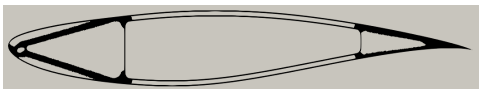

Figure 17: Weight reduction target: 25%.

Regarding the optimal reduction target, following the same explanation for the optimisation of the general case study, the 25% target seems to be adequate (Figure (17)). Despite the general layout has changed, an analog truss structure as in the previous studied case was obtained (note the results in Figure (18)).

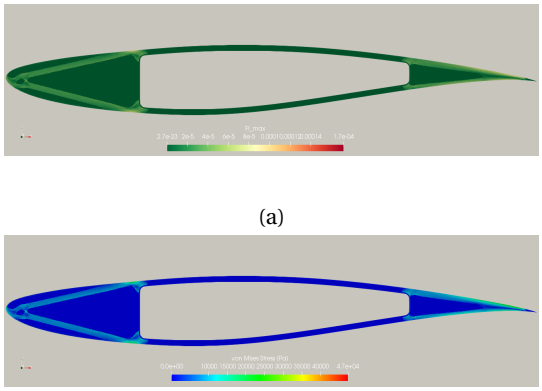

(a)

(b)

Figure 18: (a) Failure index distribution and (b) von Mises stress distribution for the optimisation of the second case study for a 25% mass reduction.

The main lessons learnt from the study are: (i) the well-behaved output obtained by the sequential coupling; (ii) the noticeable influence that a single parameter has in the final layout, using the BESO method; (iii) and that, for 2D aerofoils only aerodynamically loaded, a high percentage of material removal can be obtained.

V Conclusions

This research aimed at coupling both aerodynamic and structural designs of aerofoils using efficient optimisation tools such as aerodynamic shape optimisation and topology optimisation. Firstly, based on the analysis carried out along the process to reach the stated target, it allowed to conclude that this field has capabilities to develop highly-influential new designs.

In terms of the aerodynamics, the study has shown that, for very small geometric modifications, noticeable changes in the behaviour were found. For instance, the shockwave was softened even for small shape changes of 0.1%c, leading to considerable drag reductions of 13.9% for $M = 0.729$ and $\alpha = 2.31°$ and 29.04% for $M = 0.730$ and $\alpha = 2.79°$. Then, the research has shown that, by improving the aerodynamic behaviour of the aerofoil, the structure stress state is alleviated.

Discussing then the inner topology distribution, the BESO method has shown to be a robust and practical optimisation method as it not only removes material from the geometry but it also adds and redistributes it along aiming at the better and compliant design. Therefore, this tool can be considered very powerful

not because of the numerical and computational resources but the free-choice design it offers.

Future Work and Recommendations

As future work, it is recommended to expand the case described in this work, beginning with the creation of an flight envelope including the different sets of aerodynamic-modified geometries for a 2-D aerofoil. Next and, in order to start from a more realistic and functional study, new geometrical constraints should be defined. Then, the case can be expanded to the tridimensional space, thus a wing and all the systems it is related to. By doing so, a noticeable increase in difficulty of the computational process will be required but, using the knowledge of the open-source community and the commercial tools, these drawbacks can be surpassed.

References

[1] T. A. Zang, "Airfoil/Wing Optimization," *Encyclopedia of Aerospace Engineering*, pp. 1–11, 2010.

[2] S. Bagy, B. Mohammadi, M. Meheut, M. Lallia, and P. Coat, "Aerodynamic shape optimization of aircraft engine nozzles based on Computer-Aided Design," no. January, pp. 1–14, 2020. in Proceedings of the AIAA SciTech 2020 Forum, Orlando, FL, 2020.

[3] I. Tyapin, M. Sandberg, M. Kokkolaras, A. Lundbladh, and O. Isaksson, "Jet engine design optimization using a knowledge-based master model," *Proceedings of the ASME Turbo Expo*, vol. 7, no. PARTS A AND B, pp. 41–47, 2012.

[4] L. Zhu, N. Li, and P. R. Childs, "Light-weighting in aerospace component and system design," *Propulsion and Power Research*, vol. 7, no. 2, pp. 103–119, 2018.

[5] P. R. Spalart and S. R. Allmaras, "One-equation turbulence model for aerodynamic flows," *Recherche aerospatiale*, no. 1, pp. 5–21, 1994.

[6] F. Palacios, T. D. Economon, A. C. Aranake, S. R. Copeland, A. K. Lonkar, T. W. Lukaczyk, D. E. Manosalvas, K. R. Naik, A. Santiago Padrón, B. Tracey, A. Variyar, and J. J. Alonso, "Stanford university unstructured (SU2): Open-source analysis and design technology for turbulent flows," *52nd Aerospace Sciences Meeting*, no. January, pp. 1–33, 2014.

[7] D. J. Mavriplis and M. Castagne, "Adjoint-Based Sensitivity Analysis for Computational Fluid Dynamics," tech. rep., Department of Mechanical Engineering, University of Wyoming, Laramie, WY USA.

[8] S. K. Nadarajah and A. Jameson, "A comparison of the continuous and discrete adjoint approach to automatic aerodynamic optimization," *38th Aerospace Sciences Meeting and Exhibit*, 2000.

[9] T. D. Economon, J. J. Alonso, T. Albring, and N. R. Gauger, "Adjoint formulation investigations of benchmark aerodynamic design cases in SU2," *35th AIAA Applied Aerodynamics Conference, 2017*, no. June, pp. 1–13, 2017.

[10] T. W. Sederberg and S. R. Parry, "Free-Form Deformation of Solid Geometric Models.," *Computer Graphics (ACM)*, vol. 20, no. 4, pp. 151–160, 1986.

[11] S. N. Skinner and H. Zare-Behtash, "State-of-the-art in aerodynamic shape optimisation methods," *Applied Soft Computing Journal*, vol. 62, pp. 933–962, 2018.

[12] P. R. Lancaster and D. Mitchell, *Advanced Solid Mechanics*. No. March, 1980.

[13] X. Huang and Y. M. Xie, "Convergent and mesh-independent solutions for the bi-directional evolutionary structural optimization method," *Finite Elements in Analysis and Design*, vol. 43, no. 14, pp. 1039–1049, 2007.

[14] O. M. Querin, G. P. Steven, and Y. M. Xie, "Evolutionary structural optimisation (ESO) using a bidirectional algorithm," *Engineering Computations (Swansea, Wales)*, vol. 15, no. 8, pp. 1031–1048, 1998.

[15] North Atlantic Treaty Organization. Advisory Group for Aerospace Research and Development. Fluid Dynamics Panel. Working Group 04., "Experimental data base for computer program assessment," tech. rep., 1979.

[16] S. R. Allmaras, V. Venkatakrishnan, and F. T. Johnson, "Farfield boundary conditions for 2-D airfoils," *17th AIAA Computational Fluid Dynamics Conference*, no. June, pp. 1–15, 2005.

[17] KTH Royal Institute of Technology in Stockholm, "Boundary Conditions." Academic Resources, [Online; last accessed 2020-07-01].

[18] N. U. Guide, T. N-dimensional, I. O. Arrays, T. A. Interface, C. Rules, and O. Ufunc, "NumPy Reference," 2020.

[19] SciPy Community, "SciPy Reference Guide 0.7," p. 1229, 2013.

[20] G. Yang, A. Da Ronch, J. Drofelnik, and Z. T. Xie, "Sensitivity assessment of optimal solution in aerodynamic design optimisation using SU2," *Aerospace Science and Technology*, vol. 81, pp. 362–374, 2018.

[21] A. Díaz and O. Sigmund, "Checkerboard patterns in layout optimization," *Structural Optimization*, vol. 10, no. 1, pp. 40–45, 1995.